Japanese Journal of Applied Physics
Vol. 43, No. 9A, 2004, pp. 6268–6273

Effect of Grain Curvature on Nano-Indentation Measurements of Thin Films

Kuang-Yue TSAI, Tsung-Shune CHIN* and Han-Ping D. SHIEH[1]

Department of Materials Science and Engineering, National Tsing Hua University, 101, Sec-2. Kuang-Fu Rd., Hsinchu 30043, Taiwan
[1]*Institute of Electro-Optical Engineering, National Chiao-Tung University, 1001, Ta-Hsueh Rd., Hsinchu 30010, Taiwan*

(Received February 6, 2004; revised May 6, 2004; accepted May 10, 2004; published September 9, 2004)

Grain curvature effect on the measurement of nano-indentation has been observed for the first time, taking VO_2 thin film as an example. As the grain size of thin film is comparable to the diameter of indenter tip, the maximum penetration depths under the same maximum load (P_{max}) vary and lead to deviations in estimated hardness and Young's modulus. Under the same P_{max}, larger penetration depth leads to a larger projected area, and a decrease in hardness. The large deviation of stiffness, affected by surface roughness under low P_{max}, produces fluctuation of Young's modulus. Increase in penetration depth diminishes the roughness effect so that deviations in penetration depths dominate the variations in Young's modulus. The hardness and Young's modulus curves measured at lowest penetration depth, being thought to be free from effect of grain curvature, coincide very well to the curves measured by continuous stiffness measurements mode. [DOI: 10.1143/JJAP.43.6268]

KEYWORDS: Nano-indentation, Hardness of thin film, Young's modulus of thin film, VO_2, Vanadium dioxide, Grain curvature effect

1. Introduction

During the miniaturization of electronics and optical devices constructed by layered structure, such as optical and magnetic data-storage, surface and near-surface tribological and mechanical properties of thin films dominate the performances of materials. However conventional testing methods for bulk materials are not available in the measurement of mechanical properties of thin films at sub-micron scale. Among the new testing methods for sub-micron materials, nano-indentation has been a promising technique applicable in measuring the mechanical properties of thin films at a very small scale.[1–6] The penetration depths and applied stress are monitored simultaneously during the indenting. From the load-unload data, the hardness and Young's modulus of thin films are derived with a method elucidated by, for instance, Oliver and Pharr.[2]

As the indentation depth is small, the measured mechanical properties are determined by the intrinsic film properties. While the indentation depth increases to a certain fraction of film thickness, the measured value will be affected by the substrate. During the analyses, some important factors should be taken into consideration such as natural behavior and thickness of the films and relative hardness between the substrate and the thin film. These factors can be used to determine the maximum indentation depth regardless of substrate effect and, furthermore, real mechanical properties of thin film can be extracted.

However, how the grain curvature of thin film affects the nano-indentation measurements remains unveiled when the grain size is close to the area of indenter tip. We aimed to study the effect of grain curvature on the measurement of thin film by nano-indentation, taking VO_2 thin film as a sample. On the other hand, the effects of grain curvature on different measurements, using the monotonic indentation mode and continues stiffness (CSM) mode, are also delineated. In the meantime mechanical properties of VO_2 thin film are also determined.

2. Experimental

VO_2 films were deposited by rf magnetron sputtering with a V_2O_5 target, 2-inch in diameter. Targets were prepared by powder compaction and then sintered at 650°C for 30 min and cooled down to room temperature, both in air. The distance between the substrate and the target for sputtering was 10 cm. The vacuum chamber was evacuated to 10^{-5} Torr and then back-filled with a mixture of Ar and oxygen to a certain total gas pressure. In order to maintain a sputtering pressure measured by using a capacitance manometer (MKS Baratron gauge), Ar and oxygen were pre-mixed in a small chamber at a positive pressure before being led into the vacuum chamber. During deposition, the gas pressure in pre-mixed chamber and the processing chamber pressure were 15 kgf/cm^2 and 30 mTorr, respectively. The substrate temperature (T_s) and sputtering power were kept at 400°C and 90 W, respectively, under an oxygen flow ratio (R_{fo}) 0.015, where $R_{fo} = (f_{O_2})/(f_{O_2} + f_{Ar})$ and f is the flow rate of the gas in sccm. Well-cleaned fused silica glasses were used as the substrates that were heated by irradiation lamps during sputtering, and the temperature was measured *in-situ* by using a thermocouple. Scanning electron microscopy (SEM) was used in the measurement of surface morphology, microstructures and thickness of films. Atomic force microscopy (AFM) was used to scan the topography of thin films. Because the deposition rate of films was kept at 100 nm/h, the thickness of all films was 400 nm by controlling the deposition time. X-ray diffraction (XRD) patterns, used as phase identification, were recorded by a diffractometer (D/max-IIB, Rigaku) in the 2θ range of 10–50°. The crystalline phase of as-deposited films is identified as VO_2, as shown in Fig. 1, as the partial pressure ratio of oxygen is 1.5%.

Nano-indentation measurements were accomplished by an MTS Nano Indenter XP System with a Berkovich Diamond tip. The depth resolution of this system is noted to reach 0.1 nm. The samples were tested by a monotonic load-unload mode under different maximum loads as well as a CSM mode for comparison. It took 15 s for loading process in each test, so that the increasing rate of loading was set the same for each test under the same maximum load. The CSM mode was carried out with loading function containing both monotonic and AC signal of 45 Hz with 2 nm displacement.

*Corresponding author. E-mail address: tschin@mx.nthu.edu.tw

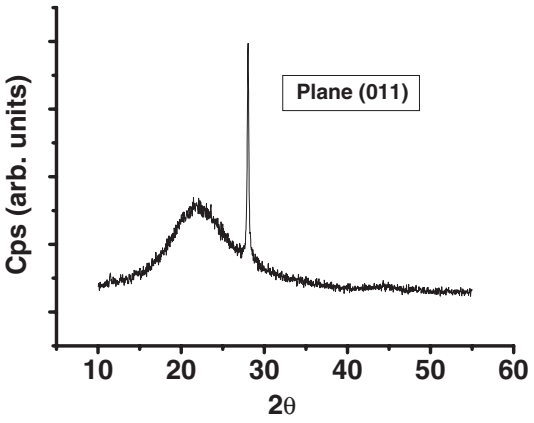

Fig. 1. XRD analysis of the VO_2 film prepared under partial pressure ratios of oxygen 1.5%.

3. Theory

During the tests, the hardness of sample can be expressed as

$$H = \frac{P_{\max}}{A} \tag{1}$$

where $P_{\max}$ and A are the maximum loading of the indenter and projected contact area during indenting, respectively. The relationship between Young's modulus of thin film, E_{tf}, and the indenter, E_{i}, is given by the following equation

$$\frac{1}{E_{\mathrm{eff}}} = \frac{1-\upsilon_{\mathrm{i}}{}^2}{E_{\mathrm{i}}} + \frac{1-\upsilon_{\mathrm{tf}}{}^2}{E_{\mathrm{tf}}} \tag{2}$$

where υ_{i} and υ_{tf} are Poisson ratios of the indenter and thin film, respectively. The effective elastic modulus, E_{eff}, is given by the equation:[4)]

$$E_{\mathrm{eff}} = \frac{1}{\beta}\frac{\sqrt{\pi}}{2}\frac{S}{\sqrt{A}} \tag{3}$$

where S and β are the stiffness and the geometry constant of the indenter, repectively. ($\beta = 1.034$ for the Berkovich tip) From eq. (2), the Young's modulus of a thin film can be transformed to the following equation.[5)]

$$E_{\mathrm{tf}} = \left(1-\upsilon_{\mathrm{tf}}{}^2\right)\left[\frac{1}{E_{\mathrm{eff}}} - \frac{1-\upsilon_{\mathrm{i}}{}^2}{E_{\mathrm{i}}}\right]^{-1} \tag{4}$$

The Poisson ratios f the diamond indenter and thin film are 0.07 and 0.25 (assumed), repectively. Because the Young,s modulus of diamond indenter is 1140 GPa which is considered to be much larger than the thin film, we can get the relationship between Young's modulus and Passion ratio of thin film and the indenter as

$$\left[\frac{(1-\upsilon_{\mathrm{tf}}{}^2)}{E_{\mathrm{tf}}}\right] \gg \left[\frac{(1-\upsilon_{\mathrm{i}}{}^2)}{E_{\mathrm{i}}}\right] \tag{5}$$

Therefore, the eq. (4) can be further simplified as the following

$$E_{\mathrm{tf}} = \frac{\sqrt{\pi}}{2}\frac{(1-\upsilon_{\mathrm{tf}}{}^2)S}{\beta\sqrt{A}} \tag{6}$$

The projected contact area, A, can be expressed by the polynomial of contact depth, h_{c},:[7)]

$$\begin{aligned} A(h_{\mathrm{c}}) = {} & m_0 h_{\mathrm{c}}{}^2 + m_1 h_{\mathrm{c}} + m_2 h_{\mathrm{c}}{}^{1/2} + m_3 h_{\mathrm{c}}{}^{1/4} \\ & + m_4 h_{\mathrm{c}}{}^{1/8} + m_5 h_{\mathrm{c}}{}^{1/16} + m_6 h_{\mathrm{c}}{}^{1/32} \\ & + m_7 h_{\mathrm{c}}{}^{1/64} + m_8 h_{\mathrm{c}}{}^{1/128} \end{aligned} \tag{7}$$

For perfect Berkovick tip, $m_0 = 24.5$ and other terms are all zero. For our system calibrated by MTS Inc., only m_1, m_2, m_3, m_4 are given and they are 322.49, 63.008, 1.4940 and 31.523, respectively. On the other hand, the contact depth, h_{c}, can be estimated from

$$h_{\mathrm{c}} = h_{\max} - \varepsilon\frac{P_{\max}}{S} \tag{8}$$

where $h_{\max}$ is the maximum depth of penetration and ε is the geometry constant which is 0.75 for Berkovick tip. The unloading stiffness, S, can be established by differentiating unloading curve at $h_{\max}$, as shown below:

$$S = \frac{dp}{dh}(h = h_{\max}) \tag{9}$$

4. Results and Discussion

Mechanical properties of VO_2 thin film and glass substrate were both measured by CSM mode. The hardness and Young's modulus of the substrate at different depths, as shown in Fig. 2, are almost constant values of 8 GPa and 70 GPa, respectively. The deviations of the ten measurements are within ± 1 GPa and ± 5 GPa for hardness and Young's modulus, respectively. Mechanical properties of VO_2 films with thickness 400 nm, as shown in Fig. 3, shows that the Young's modulus and hardness of VO_2 thin film are kept at constant values of about 130 GPa and 12.5 GPa, respectively, until the indentation depth reaches about 80 nm. Beyond this depth, both Young's modulus and hardness decrease slowly, attributed to the substrate effect. The critical depth beyond which the mechanical properties of thin film will be influenced by the substrate is about 80 nm or 20% of film thickness.

Under the same load, the maximum penetration depth should be the same. However, as shown in Figs. 4 and 5, the deviations in penetration depths reach as much as 20 nm, much larger than the resolution of depth. The deviation in penetration depth also leads to over 30% of variations in

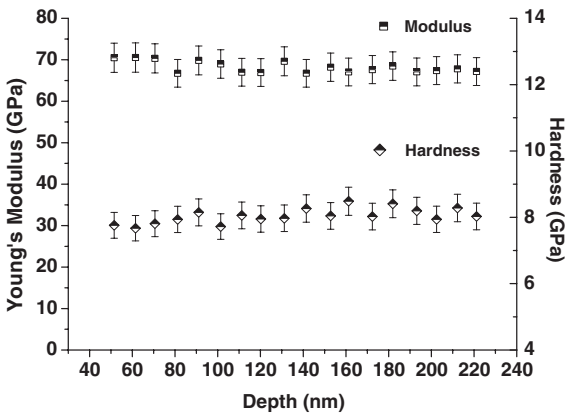

Fig. 2. Hardness and Young's modulus of corning glass substrate measured by CSM mode.

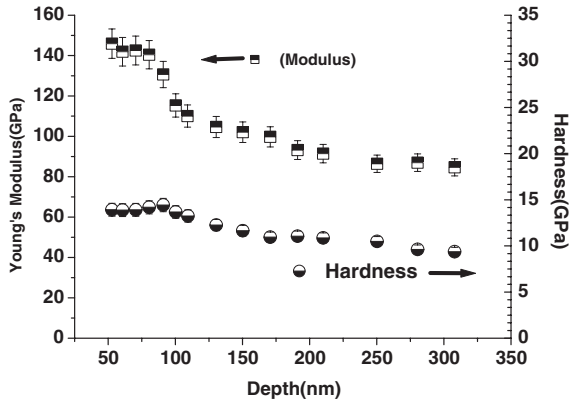

Fig. 3. Hardness and Young's modulus of VO_2 film with 400 nm thickness measured by CSM mode.

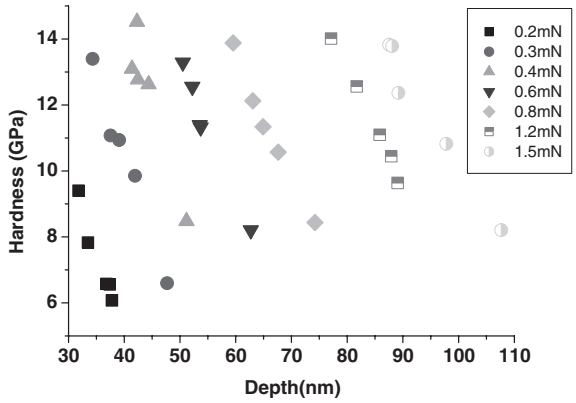

Fig. 4. Hardness of VO_2 film with 400 nm thickness measured under different P_{max}.

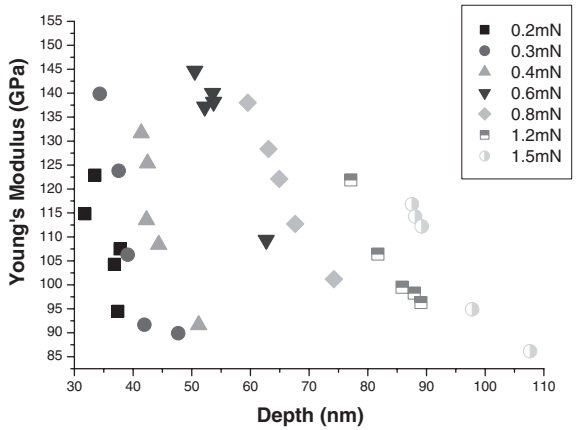

Fig. 5. Young's modulus of VO_2 film with 400 nm thickness measured with different P_{max}.

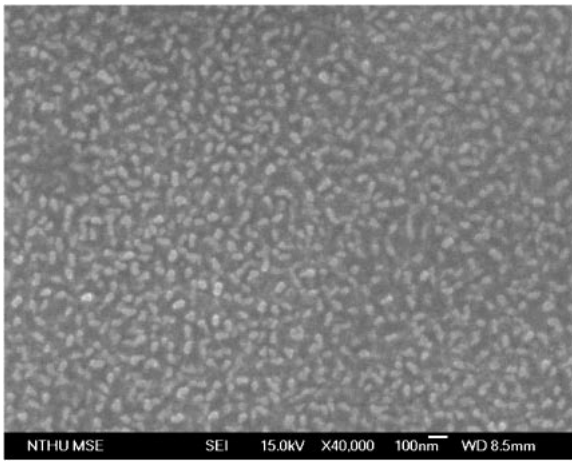

Fig. 6. A typical SEM micrograph of VO_2 film under study.

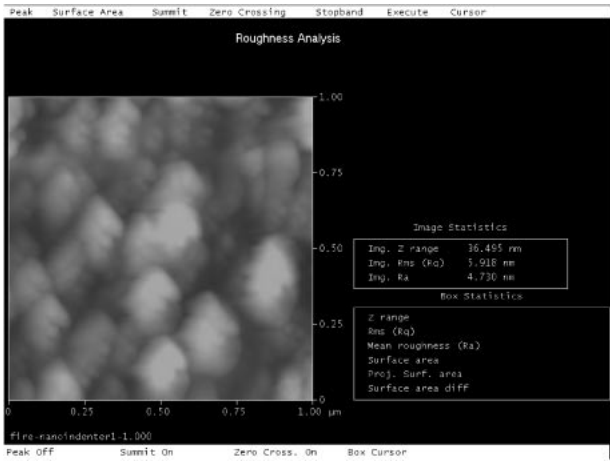

Fig. 7. Roughness of VO_2 film scanned by AFM.

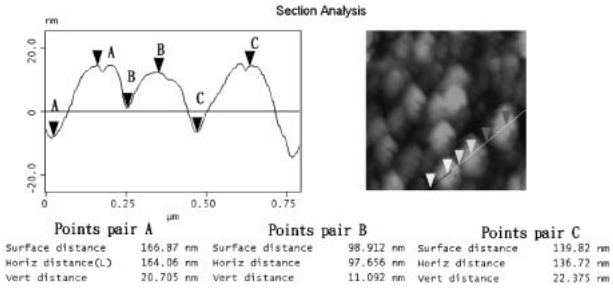

Fig. 8. Section analysis from topography scanned by AFM. It shows the curvature of surface bump (grain) being about 80–120 nm.

both hardness and Young's modulus. As the maximum indentation depth increases under the same maximum loading, both hardness and modulus decrease. We attributed the phenomenon to the roughness as the grain size of thin film is comparable to the tip radius. The typical SEM micrograph of our sample, as shown in Fig. 6, reveals that the grain size of this sample is about 100–200 nm, similar to the topography examined by AFM, as shown in Figs. 7 and 8. The grain size is comparable with the tip radius of Berkovich tip that is around 50–100 nm. The roughness of thin films is about 20 to 40 nm. As shown in Table I, the deviations of penetration depths under the same maximum load are no more than 40 nm that is close to the maximum roughness of the thin film.

The surface of the film with a roughness of current study can be thought to be composed of many bumps. The early portion of the load curve is associated with the first contacting location between tip edge and a bump. As shown

Table I. Minimum penetration depth, deviation of h_{max} and ε (P_{max}/S) under different loads (unit:nm).

Load (mN)	20	30	40	60	80	120	150
Minimum penetration depth	31.8	34.3	41.4	46.5	59.5	79.1	87.5
h_{max} variation (nm)	6.1	13.4	9.8	12.5	14.7	11.3	19.5
ε (P_{max}/S) variation (nm)	1.2	2.6	2.5	0.89	0.8	1.8	2.7

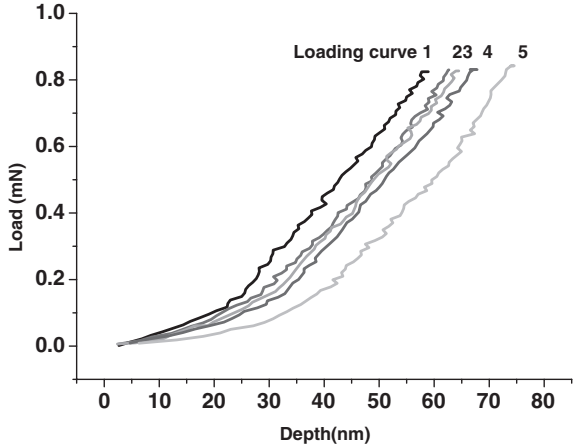

Fig. 9. Load-depth curves of loading processes under $P_{max} = 0.8$ mN measured by monotonic tests.

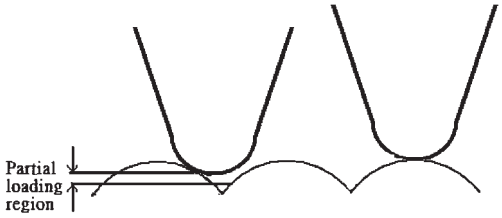

Fig. 10. Loading processes involving the tips touching at different places of a grain with small curvature.

in Fig. 9, The loading curves of the tests under a load 0.8 mN indicate that the test of deeper penetration depth has a smoother increase in the early portion of loading and this trend is the same in every set of tests under different loads. The slower loading and larger penetration rate of the early portion reveal smaller retardation for tip advancement. Smaller retardation is caused by partially loading of tip. As shown in Fig. 10, only left part of the left tip contacts the surface of a bump, so that the retardation of early loading portion should be much lower than that in other cases in which the right tip touches the top of bumps first. Furthermore, the distance between the first touching point in the former situation and the location where the maximum load can be sustained should be large, leading to deeper measured penetration depth. On the other hand, for the film with the same roughness but larger grain size, the surface curvature of grains is large so that the indenter can be thought to touch the film surface uprightly everywhere, as shown in Fig. 11. Furthermore, the depths from first

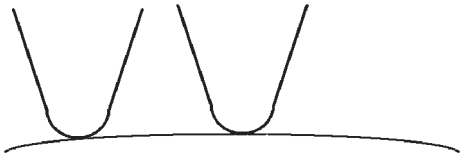

Fig. 11. Loading processes involving the tips touching at different places of grain with a large curvature.

Table II. Average stiffness, stiffness deviation and deviation ratios of stiffness under different loads.

Load (mN)	20	30	40	60	80	120	150
Average stiffness	20444	22179	23193	33952	36005	38335	42220
Variation of stiffness	3278	4548	4125	2886	1657	2600	3079
Variation ratio	16%	21.5%	17.7%	6.7%	4.6%	6.8%	6.9%

Fig. 12. Surface-tip relationships at different penetration depths.

touching point to the location with maximum load are almost the same everywhere.

The deviation ratio of stiff, S_d, can be taken as a measurement of tip immersion in thin film, and is defined as

$$S_d = 2(S_{max} - S_{min})/(S_{max} + S_{min}) \quad (10)$$

where S_{max} and S_{min} are the maximum and minimum values of stiffness under different loads. As listed in Table II, the stiffness deviation ratios from lower loads are larger than those from larger loads. It is reasonable that, for the smaller loading, the contact areas of film and tip are affected by the roughness, as shown by the left tip of Fig. 12, and result in largerr fluctuations of both unloading process and stiffness. However, once the tip proceeds deeper and is immersed more by the film, as shown by the right tip of Fig. 12, the effect of surface roughness becomes very small so that the variation ratio of stiffness becomes smaller and the shape of unloading curves, as shown in Fig. 13, should be identical regardless of loading curves. For the load of 120 and 150 mN, the slight increase of variation ratio is caused by the substrate effect that is sensitive to penetration depth.

From eqs. (1) and (6), it is clear that both hardness and Young's modulus are functions of projected area that is also a function of contact depth h_c. From eq. (8), it is clear that h_c is also the function of h_{max}, P_{max}, and S. If the variation of h_{max} is too large, it will cause large variations of both hardness and modulus. From eq. (1), under the same maximum load, the hardness is inversely proportional to the projected contact area. Table I shows values of the 1st and 2nd terms in eq. (8) from tests under different P_{max}. The variations of 2nd terms in eq. (8), for each test, are much smaller than the 1st terms so that the variations of h_c are

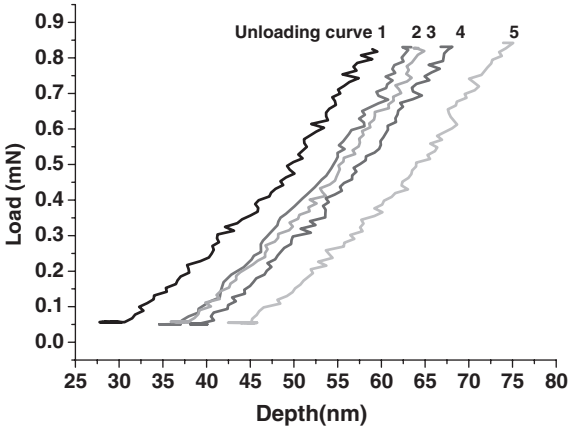

Fig. 13. Load-depth curves of unloading processes under $P_{max} = 0.8$ mN measured by monotonic tests.

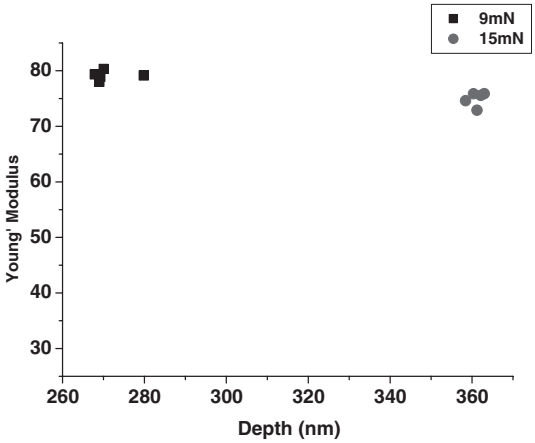

Fig. 15. Young's modulus from tests under $P_{max} = 9$ and 15 mN.

mainly arisen from different h_{max} of each measurement. The increasing of penetration depth, h_c, will lead to larger projected area of tip. Therefore, the hardness is underestimated and, as Fig. 4 shows, decreases as penetration depth increases under the same P_{max}.

Young's modulus, as shown in eq. (6), is proportional to the stiffness and inversely proportional to the square root of area. The larger penetration leads to larger h_c, larger projected area and, furthermore, smaller Young's modulus. For the tests with smaller loads, large variations of stiffness result in large fluctuations of Young's modulus for some tests with deeper penetration depths. For example, the larger depth in test at penetration depths of 33.8 nm under 0.2 mN leads to larger projected area and smaller hardness than those in test at 31.8 nm. Actually, much larger stiffness of the test at 33.8 nm results in the inverse increase of modulus although its depth and projected area are larger. The inverse increase only appears in the low load region because of large fluctuation in stiffness.

The mechanical properties at deeper depths, being free from roughness effect, show lower variation ratios of both mechanical properties. Although the depth variations under constant load are almost the same in all tests, comparing the variations at depths below 100 nm, the mechanical properties at depths 280 and 360 nm, as depicted in Figs. 14 and 15,

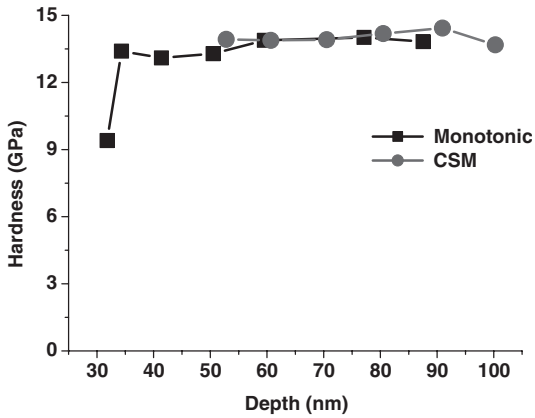

Fig. 16. Comparison of hardness measured by CSM and monotonic tests with lowest penetration depths.

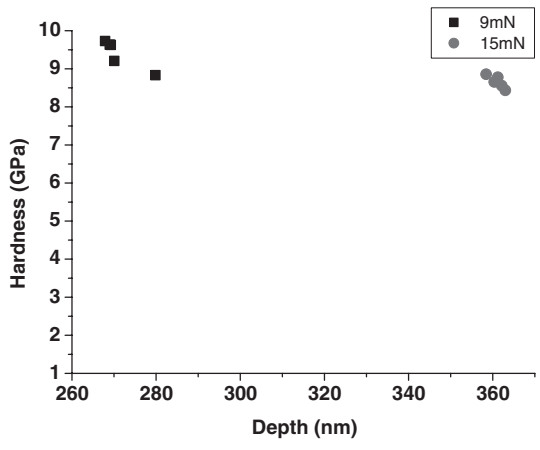

Fig. 14. Hardness from tests under $P_{max} = 9$ and 15 mN.

show smaller variation ratios of both mechanical properties and imply that the ratio of (depth variation)/(depth) is the main cause of variations in both Young's modulus and hardness under the same load. The mechanical properties at deeper penetration depths also tend to be much closer to the substrate properties.

Based on our assumption, the tests with lowest depths are thought to be free of partial loading and the tips indent surface uprightly. The comparison of results from CSM test mode and the plot composed of the tests with lowest penetration depths under each load, as shown in Figs. 16 and 17, shows that the large fluctuations of both Young's modulus and hardness at low depths prove the existence of surface roughness effect on the stiffness and estimation of effective projected area. The curves measured by both CSM and monotonic measurement show high similarity on both hardness and Young's modulus between depths 50 to 100 nm. The hardness almost keeps constant between depth 50–100 nm. The larger modulus drops at depth about 70 nm may be caused by the lack of data of monotonic measurement at corresponding depths. All points coincide well to each other regardless those of the 70 nm data. The decay of Young's modulus starting from depth 75 nm, caused by the substrate effect, is observed both in CSM and monotonic measurements. The reason why all tests measured by CSM

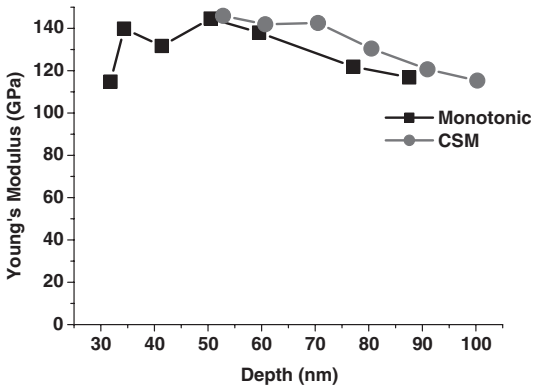

Fig. 17. Comparison of Young's modulus measured by CSM and monotonic tests with lowest penetration depths.

do not show the curvature effect is not clear. It may arise from the low sensitivity on the phase lag of input and feedback displacement signal used in the calculation of stiffness. Once the phase lag is detected, the tip has completely loaded onto the surface making identical starting point in depth of each test. Furthermore, no more depth variation effect occurs on the calculation of Young's modulus and hardness.

5. Conclusions

The grain curvature effect on the nano-indentation measurement of thin films has been observed by taking VO_2 thin film as an example. By continuous stiffness measurement, the hardness and Young's modulus of VO_2 film are 14 GPa and 140 GPa, respectively, being reported here for the first time in literatures. The critical depth of VO_2 film with thickness 400 nm is about 80 nm, or 1/5 of film thickness. With monotonic load measurement, under constant load, the variations of penetration depths also lead to large variations in both Young's modulus and hardness. Under the same loading, the larger penetration depth leads to smaller hardness because of larger estimated projected area. The larger variations of stiffness, especially in tests of shallow penetration depths, compensate the increase of projected area and cause fluctuations in Young's modulus. The variations of stiffness decrease as the penetration depths increase. Therefore, Young's modulus also decreases because of large projected area. These phenomenons are concluded to arise from the effect of grain curvature that is comparable with the tip radius. The plots of Young's modulus and hardness, composed of data at lowest penetration depths under different loads, coincide well with the data measured by CSM mode, implying that these tests are free from the curvature effect of grain.

Acknowledgements

This work was supported by the Ministry of Education of the Republic of China with the Academic Center of Excellence in "Photonics Science and Technology for Tera Era" under contract No. 89-E-FA06-1-4 and National Science Council of the Republic of China, under Grant No. NSC 91-2120-M007-001 and NSC 92-2120-M007-006.

1) P. J. Burnett and D. S. Rickerby: Thin Solid Films **148** (1987) 41.
2) W. C. Oliver and G. M. Pharr: J. Mater. Res. **7** (1992) 1564.
3) S. Anders, D. L. Calanhan, G. M. Pharr and T. J. Tsui: Surf. Coat. Technol. **94** (1997) 189.
4) G. M. Pharr: Mat. Sci. Eng. A **253** (1998) 151.
5) T. H. Fang and W. J. Chang: Microelectron. Eng. **65** (2003) 231.
6) D. W. Stollberg, J. M. Hampkian, L. Riester and W. B. Carter: Mater. Eng. A **359** (2003) 112.
7) A. V. Kulkarni and B. Bhushan: Mater. Lett. **29** (1996) 221.